AGU ADVANCING EARTH AND SPACE SCIENCE

Geophysical Research Letters

RESEARCH LETTER
10.1029/2020GL088455

Compaction-Driven Fluid Localization as an Explanation for Lower Crustal Electrical Conductors in an Intracontinental Setting

Matthew J. Comeau[1], Michael Becken[1], James A. D. Connolly[2], Alexander V. Grayver[3], and Alexey V. Kuvshinov[3]

[1]Institut für Geophysik, Universität Münster, Münster, Germany, [2]Institute für Geochemie und Petrologie, Swiss Federal Institute of Technology (ETH), Zürich, Switzerland, [3]Institute of Geophysics, Swiss Federal Institute of Technology (ETH), Zurich, Switzerland

Key Points:
- Electrical resistivity models across a compressive intracontinental region image a pattern of low-resistivity zones in the lower crust
- The pattern is consistent with hydrodynamic stagnation of crustal fluids due to thermally activated compaction
- The results demonstrate that compaction processes, rather than lithological structure, control the regional lower crustal fluid flow

Supporting Information:
- Supporting Information S1

Correspondence to:
M. J. Comeau,
matthew.comeau@uni-muenster.de

Citation:
Comeau, M. J., Becken, M., Connolly, J. A. D., Grayver, A. V., & Kuvshinov, A. V. (2020). Compaction-driven fluid localization as an explanation for lower crustal electrical conductors in an intracontinental setting. *Geophysical Research Letters*, *47*, e2020GL088455. https://doi.org/10.1029/2020GL088455

Received 14 MAY 2020
Accepted 4 SEP 2020
Accepted article online 28 SEP 2020

Abstract We present electrical resistivity models, derived from magnetotelluric data, of the crust beneath the Bulnay region, Mongolia. They reveal that the lower crust contains a pattern of discrete zones (width of ~25 km) of low resistivity (<30 Ωm). Such features may be an effect of unaccounted-for electrical anisotropy. However, when anisotropy is considered in the modeling, the features remain. We investigate an alternative explanation, based on a conceptual model of fluid localization and stagnation by thermally activated compaction, and demonstrate it is compatible with the observed low-resistivity zones. The model explains the location, shape, and size of the zones, with plausible values of the activation energy for lower crustal creep (270–360 kJ/mol), and a viscous compaction length on the order of 10 km. The results imply tectonic deformation and compaction processes, rather than lithological-structural heterogeneity, control the regional lower crustal fluid flow.

Plain Language Summary We collected magnetotelluric data in the Bulnay region, Mongolia, which is a compressive intracontinental region, by measuring electric and magnetic fields at the surface. Using these data, we generated high-resolution electrical resistivity models. The models image the lower crust and show that it contains discrete zones of low resistivity that have a distinct pattern. Other studies have shown that such a pattern may be an effect of ignoring electrically anisotropy. But when anisotropy is considered in the modeling the features remain nearly the same. Because of this, we investigate whether an alternative explanation can cause these features. We find that a conceptual model of fluid localization and stagnation by hydromechanical compaction is compatible with the observed pattern of the low-resistivity zones. In fact, it can explain their location, shape, and size. In addition, we use the conceptual model to determine which viscous rheology is consistent with the data. Finally, we find that estimates for hydraulic and rheological properties of the region are consistent with this explanation. This conceptual model has implications for fluid flow in the lower crust, showing that it is controlled by tectonic deformation and compaction processes, rather than lithological or structural features.

1. Introduction

Fluids play an important role in the geodynamic evolution of the continental crust. At shallow depths, much is known about their properties and presence; less is known about fluids in deep crustal settings. In the lower crust, evidence for the presence of fluids comes from both exhumed rocks and geophysical observations. Direct evidence for active metamorphism and devolitalization reactions producing a fluid phase come from fluid inclusions trapped in metamorphic minerals (e.g., Manning, 2018). Geophysical imaging can also be used to image fluids in situ. However, questions remain as to the behavior of fluids in the lower crust and mechanisms that control their motion (Connolly, 2010). For example, is fluid flow controlled by preexisting lithological-structural heterogeneities in the crust, or by stresses due to tectonic deformation?

In this study, we examine the Bulnay region of north central Mongolia, at the northern margin of the Hangai Mountains and along the eastern segments of the Bulnay fault zone. Central Mongolia, part of the Central Asian Orogenic Belt (e.g., Yin, 2010), is composed of an intracontinental plateau dominated by the Hangai block, a Precambrian microcontinent (Badarch et al., 2002; Cunningham, 2001). It is bounded by large, seismically active, strike-slip faults (Walker et al., 2007). Notably, the northern Bulnay fault has

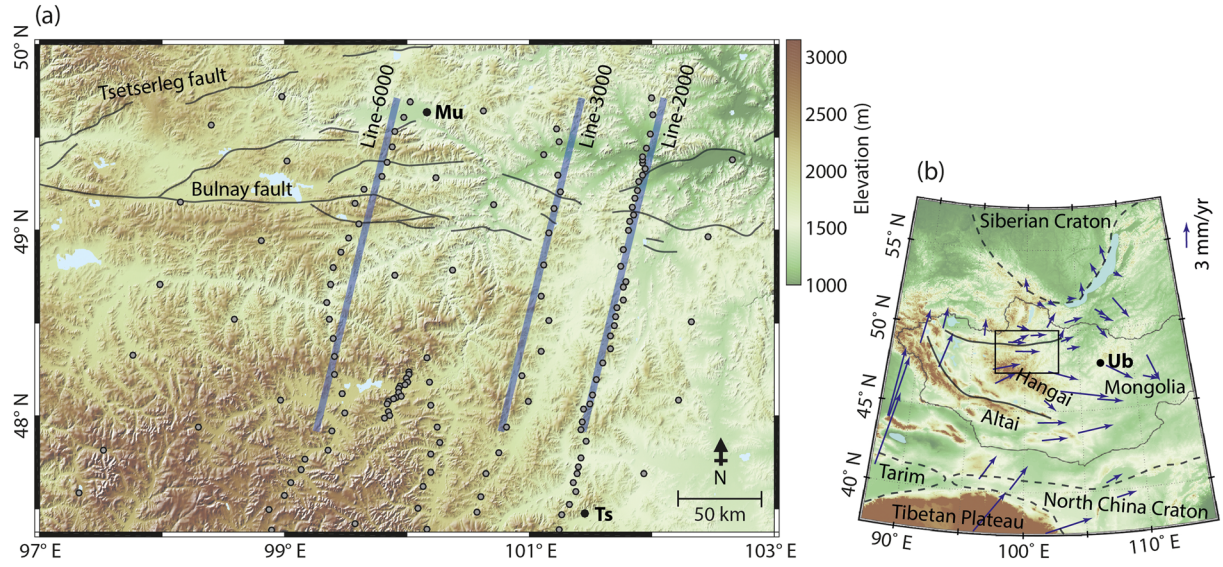

Figure 1. (a) Map of the study area in Mongolia. Magnetotelluric measurement sites (gray circles) and profiles (blue lines) are marked. The locations of the Bulnay fault segments are indicated (black lines; Walker et al., 2007). (b) The Hangai block, bounded by large faults (black; north, Bulnay; south, Gobi-Altai), is situated between the Siberian craton and the North China and Tarim cratons (dashed lines). The compressive tectonic setting is illustrated by velocity vectors (purple; Calais et al., 2003). Within the survey region (box) eastward motion is dominant. Ub = Ulaanbaatar; Mu = Murun; Ts = Tsetserleg.

experienced intracontinental earthquakes larger than magnitude 8 within the last century, despite the large distance from active tectonic margins (Calais et al., 2003; Rizza et al., 2015). Additionally, low-volume, alkali-basaltic volcanism, with little crustal assimilation, has occurred since the Cenozoic throughout the region (Barry et al., 2003).

The region occupies a unique position in central Asia between the rigid Siberian craton to the north and the North China craton to the south, which has a compressional regime due to the collision of the Indian and Eurasian plates. GPS measurements indicate northward directed movement of >10 mm/yr in northern China, whereas along the Bulnay fault eastward motion of ~3 mm/yr is detected (Calais et al., 2003).

Seismic studies suggest that the lithosphere below central Mongolia is anomalously thin (60–80 km), compared to its surroundings (150–225 km), and, in combination with a thick crust (~50 km), imply an unusually thin subcrustal lithosphere (Petit et al., 2008; Priestley et al., 2006; Welkey et al., 2018). Electromagnetic studies imaged an asthenospheric upwelling that is expected to have brought mantle material to depths of ~70 km, where it underwent decompression melting (Comeau et al., 2018; Käufl et al., 2020). This is supported by analysis of erupted xenoliths (Barry et al., 2003; Ionov, 2002) and high temperatures in the lower crust (Ionov et al., 1998).

2. Magnetotelluric Data and Electrical Resistivity Models

We analyze magnetotelluric (MT) data in the Bulnay region collected as part of a large regional array (Comeau et al., 2018, 2019, 2020; Käufl et al., 2020). Measurement sites have a spacing of <10 km along ~200 km long parallel profile segments, separated by ~50 and ~150 km (Figure 1). Broadband data were recorded with a sampling frequency of 512 Hz for several days (Figure S1 in the supporting information), providing good resolution within the crust, and allowing penetration to upper mantle depths. The MT data are high quality and have a low noise level, due to the remote measurement location.

The regional geoelectric strike was computed for all sites (Becken & Burkhardt, 2004) and a well-defined direction of N104°E was observed (Figure S2), which is approximately aligned with the trend of the Bulnay fault zone and the Hangai Mountains. Average phase tensor skew values, an indication of three dimensionality (Booker, 2014; Caldwell et al., 2004), were generally low, except regions around the fault zone, which may indicate local three-dimensional (3-D) structure (Figure S2). This analysis established that a two-dimensional (2-D) model is largely valid.

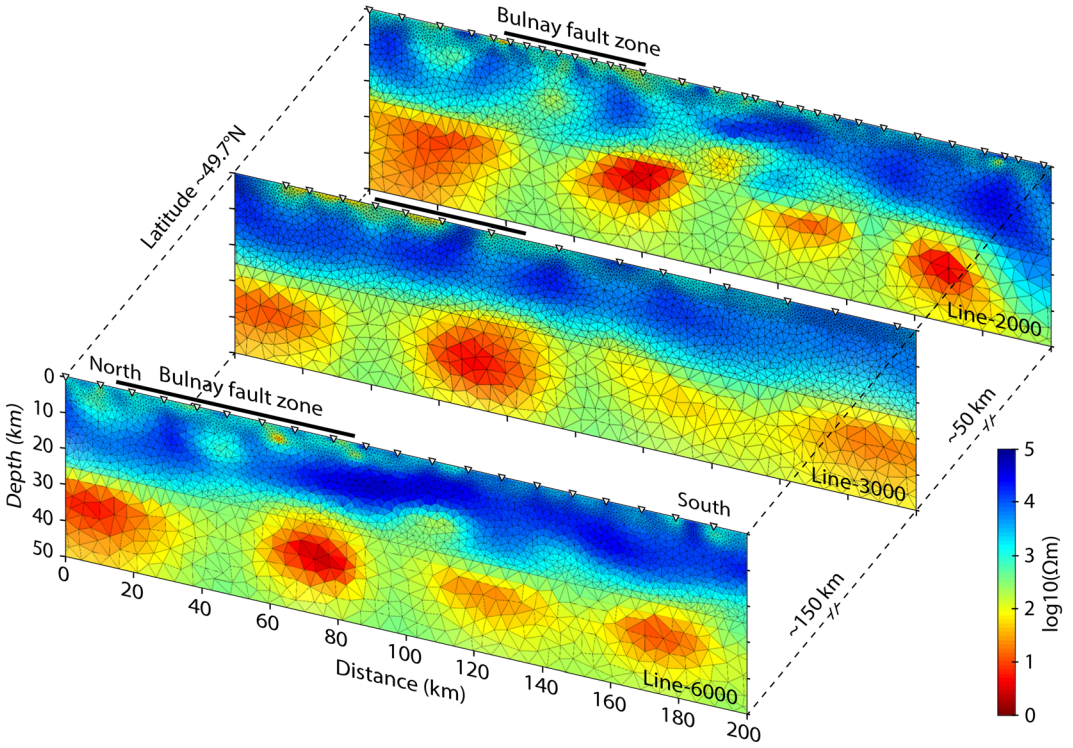

Figure 2. Electrical resistivity models obtained from the inversion of magnetotelluric data. Measurement locations are white triangles. In the lower crust, localized low-resistivity zones, with a distinct pattern of approximately equal width and separation, are observed. Near-surface features appear coincident with the diffuse Bulnay fault system (black lines; see Figure 1).

Using the MARE2DEM inversion algorithm (Key, 2016), 2-D electrical resistivity models were created by inverting both modes of the impedance tensor (Transverse Electric, TE, and Transverse Magnetic, TM), for periods in the range of 0.06–4,200 s. Topography was not included; for further inversion details, see Figure S3. Both isotropic and anisotropic models were created. For the inversion, the data were rotated to the geoelectric strike direction and projected along a perpendicular profile.

To ensure a close fit to the data, both TE and TM mode phase components were assigned an error floor of 2° and the TM mode apparent resistivity was assigned an error floor of 10%. The TE mode apparent resistivity was assigned a high error floor of 100% to reduce the influence of the static shift effect (e.g., Chave & Jones, 2012). In addition, following Becken et al. (2011), data errors were adjusted such that departures from the 2-D condition were indistinguishable within the errors, which corresponds to the downweighting of 3-D effects.

For each inversion model, the algorithm smoothly converged and the total root-mean-square (RMS) misfit was reduced to 1.00, indicating that the models fit the MT data (Table S1). Furthermore, many combinations of inversion model parameters were thoroughly investigated, and, although minor variations were observed, it was found that the main features of the model did not greatly depend on any specific choice of parameters (e.g., variations in strike angle, starting model, or mesh). In addition, model resolution and sensitivity were explored using synthetic inversions (e.g., Figure S4), which indicated the robustness of the main model features.

The upper crust (<25 km depth) appears generally very resistive (~10,000 Ωm), reflecting the cratonic setting of the Hangai microcontinent (Cunningham, 2001). Several near-surface reduced-resistivity features are coincident with the diffuse Bulnay fault system and with surface expressions of hydrothermal activity and volcanism (Comeau et al., 2018; see Hunt et al., 2012). In contrast, in the lower crust (25–50 km depth) discrete zones of low resistivity (3–30 Ωm) embedded in a moderate resistivity background (200–300 Ωm) are imaged at a depth of approximately 30–40 km (Figure 2). These oblate, elliptical features are larger than

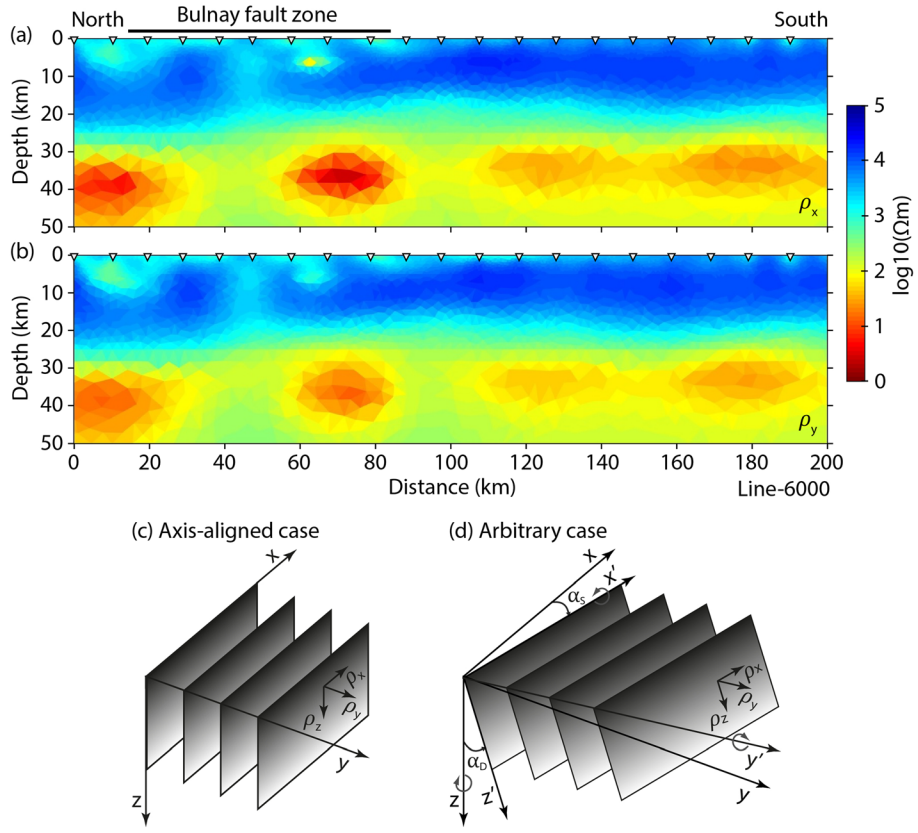

Figure 3. Anistropic electrical resistivity model along the (a) x direction and (b) y direction (Line-6000). The model shows a distinct pattern of localized low-resistivity zones, similar to the isotropic model. Comparable resistivities for both directions implies very weak electrical anisotropy. The model allows (c) axis-aligned triaxial anisotropy, anisotropy aligned with the coordinate system, rather than (d) arbitrary anisotropy, where rotations about z give an anisotropic strike (α_S), about x give a dip (α_D), and about y give a slant (α_L; not shown).

the MT site spacing. The approximate width of each zone is ~25 km, and their separation is also ~25 km. Their true vertical extent is difficult to establish because the MT method is sensitive to the top of a conductive zone and to its conductance, which can be satisfied by an equivalent combination of thickness and conductivity, indistinguishable in the data (e.g., Unsworth & Rondenay, 2012). Furthermore, their thicknesses vary, both along and across the profiles. Based on the inversion images, we estimate their thickness to be <10 km. However, they are possibly thinner features that are smeared downward by the inversion.

On each profile the low-resistivity zones appear remarkably similar, and, if the assumption of a 2-D Earth is true, they may be connected between the profiles. In fact, recent 3-D modeling results from Käufl et al. (2020) of MT array data across central Mongolia revealed laterally extended conductive structures quasi-parallel to the Bulnay fault zone (Figure S5).

An alternating sequence of resistive and conductive dykes (macroanisotropy) in 2-D isotropic resistivity models may be an effect of unaccounted-for electrical anisotropy (Heise & Pous, 2001), which can be recovered from the properties of the imaged dykes (Eisel & Haak, 1999). However, the models in this study do not show a strictly regular pattern—there are some variations in the anomalous features' widths and resistivities. Furthermore, we observed no uniform split in the phases nor regions with out-of-quadrant phases, often diagnostic of anisotropy in the data (Liddell et al., 2016; Pek & Verner, 1997) (Figure S6). Other evidence, including from seismic data, is not conclusive for crustal anisotropy. Nevertheless, we investigated whether electrical anisotropy can explain the anomalous features.

We generated electrical resistivity models that allowed axis-aligned triaxial anisotropy, that is, different resistivities in perpendicular directions aligned with the coordinate system: along and across geoelectric strike, as well as vertically. The resulting models (Figure 3) showed a very similar result to the isotropic

models—they revealed a pattern of resistive and conductive features. The ratio of horizontal resistivities (ρ_y/ρ_x) was generally less than 1.3, and no more than 2 within the conductors, signifying very low anisotropy (ρ_z was similar to ρ_y; Figure S7). The result implies that, although weak electrical anisotropy may exist, the observed resistivity pattern is not merely an artifact, and thus, axis-aligned triaxial electrical anisotropy is not a sufficient explanation for the pattern. Note that we do not consider arbitrary anisotropy, that is, anisotropy oriented at an angle to the coordinate system (e.g., Marti, 2014).

3. Results and Discussion

3.1. Fluid Content

Low resistivity in the crust can have several causes, and common explanations invoke graphite films, partial melts, or aqueous fluids (e.g., Unsworth & Rondenay, 2012). If graphite films exist beneath the Bulnay region, they would be widespread (Hyndman et al., 1993), and hence, it would be difficult to explain the observed pattern. Crustal melt is often interpreted in volcanic environments (e.g., Comeau et al., 2016; Pritchard et al., 2018). However, considering partial melt in this setting would typically have a resistivity of >3 Ωm (Comeau, 2015, and references therein; Pommier & Le Trong, 2011; Table S2), a large porosity (>10%) would be required to explain the observed conductive features. In view of these complications, we favor aqueous fluids as the simplest explanation for the origin of the anomalous low resistivity, because they do not require large porosities and are thus a more plausible match to the conceptual model discussed below.

The imaged low-resistivity zones are notably located below the brittle-ductile transition zone (BDTZ), which may be located at a depth of ~25 km in this region (Déverchère et al., 2001; Li et al., 2017; Welkey et al., 2018). This is significant because it is hypothesized that the stress gradient becomes inverted beneath the BDTZ in compressive tectonic settings, acting as a barrier to crustal fluids (Connolly & Podlachikov, 2004). Therefore, we propose that the thermally perturbed lower crust undergoes metamorphic dehydration and devolatization reactions that produce fluids, which are trapped in the lower crust, and that these fluids accumulate in localized, fluid-rich domains—causing enhanced conductivity.

To estimate the porosity (fluid-filled volume fraction) required to explain the bulk resistivity obtained from MT data, a two-phase configuration is used, considering the resistivity of the pore fluid and the rock matrix. We use the Hashin-Shtrikman (upper) bound (Hashin & Shtrikman, 1962), which assumes isolated spheres surrounded by a less resistive material, because it represents normal interconnection for lithospheric fluids (Unsworth & Rondenay, 2012). Even a small amount of fluid can cause an order of magnitude reduction in the bulk resistivity, and in the viscosity (e.g., Rosenberg & Handy, 2005), but corresponding changes in seismic velocity are small—and may go undetected (Watanabe, 1993).

In lower crustal settings, there exists evidence for ionic saline fluids with conductivities on the order of 10 S/m (Manning, 2018; Sakuma & Ichiki, 2016). Using the experimentally derived numerical model from Sinmyo and Keppler (2017), at 1 GPa (~35 km depth) and 730°C (suitable for this region) H_2O-NaCl fluids have conductivities ranging from 1.4–24 S/m, for salinities of 0.10–3.3 wt% (weight percent NaCl), which are plausible based on deep geochemical data (e.g., Sinmyo & Keppler, 2017).

Assuming a fluid conductivity of 10 S/m (corresponding to a salinity of ~1 wt%), a bulk resistivity of 30 Ωm, representative of the low-resistivity zones imaged, requires a minimum fluid content of 0.45% to explain the electrical resistivity data (Figure 4a). Whereas the background regions that are fluid poor, with an observed bulk resistivity of ~250 Ωm, require a fluid content of ~0.045%. The average bulk resistivity over the entire lower crust from the resistivity model is 125 Ωm, which can be explained by a porosity of 0.10%. Note that if the fluids are less saline—and therefore less conductive—a higher porosity is required.

3.2. Constraint on Length Scales

The spatial distribution of the low-resistivity zones is remarkably consistent with the hypothesis that the BDTZ acts as a barrier to compaction-driven expulsion of lower crustal fluids for both rheological and hydrodynamic reasons (Connolly & Podlachikov, 2004).

Thermal activation of viscous mechanisms has the consequence that the lower crust strengthens upward on the length scale ℓ_σ (Connolly & Podlachikov, 2004), which can be written as

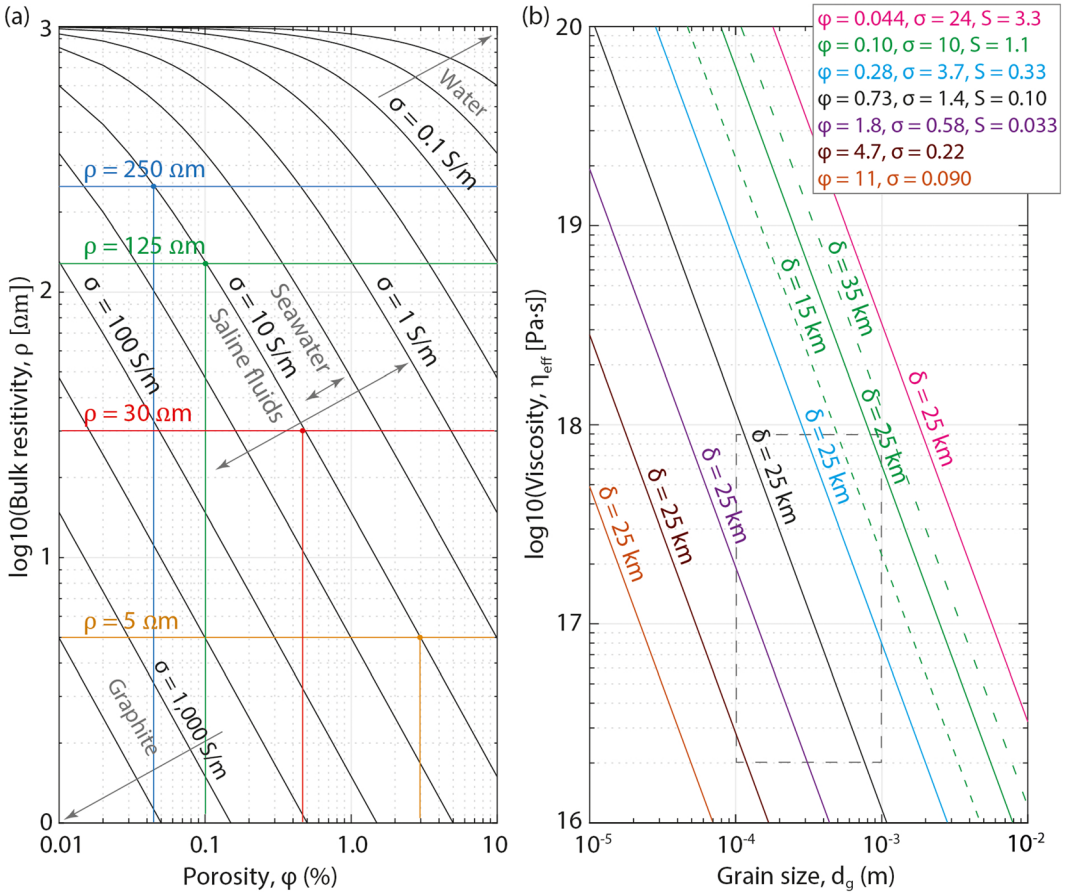

Figure 4. (a) The porosity (fluid fraction) required to explain the bulk resistivity measured from magnetotelluric data, for fluid conductivities (black lines), computed with the Hashin–Shtrikman (upper) conductivity bound (Hashin & Shtrikman, 1962). If fluid domains in the lower crust consist of saline fluids with a conductivity of 10 S/m, a measured bulk resistivity of 30 Ωm can be explained by a porosity of 0.45% (red), 250 Ωm by 0.045% (blue), and 125 Ωm by 0.10% (green). (b) The viscous compaction length (lines) for varying grain size and effective viscosity with different porosities (colors). The porosities (φ), computed from (a) for 125 Ωm, correspond to different conductivities (σ), which are controlled by the fluid salinity (S, wt% NaCl). Considering partial melt may have a conductivity <0.3 S/m (Table S2), low-salinity fluids (<1 wt%) are the most plausible match for lower crustal properties (gray box), within the conceptual model.

$$\ell_\sigma = nT^2 / \left(\frac{Q}{R} \frac{dT}{dz} \right) \tag{1}$$

where Q is the activation energy for the effective viscous mechanism, R is the gas constant, T is the temperature at depth z, and n is the stress exponent for the viscous mechanism.

Regardless of any hydrodynamic effects, upward strengthening impedes viscous compaction and tend to cause transient accumulation of metamorphic fluids in the upper portions of the crust. It has been shown numerically (Connolly, 1997; Connolly & Podladchikov, 1998) that in thermal regimes where ℓ_σ is greater than the viscous compaction length δ (Scott & Stevenson, 1984), compaction processes localize fluid on the local compaction length scale, which itself is an exponentially decreasing function of depth (Connolly & Podladchikov, 1998, 2004). In contrast, if δ is greater than ℓ_σ, the local compaction length dictates the horizontal length scale for compaction processes, and ℓ_σ controls the vertical length scale (i.e., in the direction of the thermal gradient). On the basis of these considerations, we interpret the oblate geometry of the imaged low-resistivity zones to indicate the latter regime, with $\delta \lesssim 25$ km. Given that the vertical extent of the low-resistivity zones is a particularly uncertain aspect of the inversion model, this simple rheological argumentation does not constrain ℓ_σ precisely.

A more precise constraint on ℓ_σ follows from the more elaborate hydrodynamic mechanism posited by Connolly and Podlachikov (2004), which explains the accumulation of fluids beneath the BDTZ as a quasi steady state phenomenon in compressive tectonic settings related to the viscous relaxation of upper crustal stress in the lower crust. A simple model of this mechanism (Connolly & Podlachikov, 2004) shows that the depth from the BDTZ to the center of the fluid zones is

$$\Delta z = \ell_\sigma \ln\left(\frac{s\sigma_Y}{\ell_\sigma \Delta p g}\right) \tag{2}$$

where σ_Y is the yield strength of the crust at the BDTZ, s is a geometric constant taken to be ½ for the observed near-equant geometry of the zones, Δp is the difference between the density of the fluid and solid, and g is the gravitational constant. Using the Mohr-Coulomb criterion (see Connolly & Podlachikov, 2004), the yield strength can be written as a function of the depth of the BDTZ (z_{bd}):

$$\sigma_Y = 2\Delta p g z_{bd} \tag{3}$$

This model predicts that fluids released by lower crustal metamorphism will collect in zones ≤9.2 km below the BDTZ (for $z_{bd} \leq 25$ km). This is in agreement with the observations in the Bulnay region, where the center of the fluid zones is imaged at a depth of ~35 km. For the case $\Delta z = 9.2$ km, ℓ_σ is equally 9.2 km. The corresponding activation energy (Equation 1; $dT/dz \approx 10$ K/km; Ionov et al., 1998) is 273 kJ/mol for stress exponent $n = 3$ and 364 kJ/mol for $n = 4$ (i.e., non-Newtonian behavior), suggesting the viscous mechanism is dislocation creep, characteristic of quartz-dominated rheology (Paterson & Luan, 1990), demonstrating the consistency of the compaction model. As the inversion model provides no temporal resolution, the existence of the quasi steady state hypothesized in the stagnation mechanism is speculative, but the uniform depth of the conductive zones supports the hypothesis.

3.3. Consistency With Crustal Hydromechanical Properties

The relation of the viscous compaction length to experimentally measured rock properties provides an additional test for the hypothesis that the Bulnay low-resistivity zones are consistent with compaction-induced localization of metamorphic fluids.

From the governing compaction equations (Scott & Stevenson, 1984), the viscous compaction length, ignoring order-one terms, can be generalized as

$$\delta = \sqrt{\frac{\zeta k}{\eta_f}} \tag{4}$$

where ζ is the bulk viscosity, η_f is the pore fluid viscosity, and k is the permeability. Assuming a dislocation creep mechanism (Wilkinson & Ashby, 1975), a plausible rheology for this setting (e.g., Bürgmann & Dresen, 2008),

$$\zeta = \frac{\eta_{\text{eff}}}{\varphi} \tag{5}$$

where η_{eff} is the effective viscosity and φ is the porosity. Following the theoretical Carman–Kozeny porosity-permeability relationship (Beard & Weyl, 1973; Carman, 1939),

$$k = \frac{\varphi^3 d_g^2}{c_\varphi} \tag{6}$$

where d_g is the grain size and c_φ is a material constant estimated by Carman (1939) to be on the order of 10—an estimate that has been experimentally confirmed for geological materials (Connolly et al., 2009).

Using GPS measurements and models of postseismic deformation, Vergnolle et al. (2003) determined that the viscosity of the lower crust in central Mongolia must be approximately 10^{16} to 10^{18} Pa·s, which is low compared to other crustal settings (e.g., Bürgmann & Dresen, 2008). However, it is compatible with

elevated temperatures, as inferred from petrological analysis (Ionov et al., 1998), and consistent with a weak, fluid-rich lower crust. The average grain size in the lower crust is estimated to be on the order of 10^{-4} to 10^{-3} m, based on the crustal properties and setting (Bürgmann & Dresen, 2008; Karato, 2008), which is reasonable considering petrological studies in Mongolia (e.g., Barry, 1999). Moreover, the grain size can be estimated directly from Equation 6, using an inferred lower crustal permeability (e.g., Connolly & Podladchikov, 2013) (Figure S8).

The initial uniform porosity, which existed prior to localization, is inferred to be 0.10%, based on the average resistivity of the present-day lower crust. A higher porosity—for example if fluids are less saline—necessitates a lower effective viscosity to explain the same viscous compaction length (Figure 4b). The pore fluid viscosity is assumed to be 10^{-4} Pa·s, based on experimental measurements of aqueous solutions of NaCl and KCl over a range of relevant pressures and temperatures, which show little variation (Hack & Thompson, 2011; Kestin et al., 1981).

Using a combination of the above parameters gives a viscous compaction length of $\delta \approx 25$ km (Figure 4b). This is consistent with the geophysically imaged low-resistivity zones. Although uncertain, this analysis suggests that the above estimates for crustal properties are not unreasonable and that the length scales discussed here are consistent with basic assumptions and with independent geodynamic inferences.

3.4. Sealed Fault Zone and Compaction

In the absence of compaction, repeated deformation along large-scale fault zones is expected to create drainage networks in the lower crust (Cox, 1999; Sibson, 1986). In this case, the fluids trapped beneath the BDTZ in the Bulnay region would flow laterally toward the active fault zone. However, in the compacting case, fault drainage is less effective due to decreasing fluid flow (Connolly, 2010). This is because the fault acts as a drain faster than fluid is generated, causing porosity to collapse due to compaction and low fluid pressure, and hence, hydraulic connectivity and permeability are drastically reduced. Effectively, compaction processes act to seal the fault zone, thereby preventing fluid drainage, and the consequence is that lower crustal fluid regions act independently of the fault (Connolly, 2010).

The resistivity models present an example of this effect. Although the survey area crosses a significant crustal boundary, the eastern segments of the Bulnay fault zone, it is not imaged as a strong low-resistivity zone at midcrustal depths, as expected from studies at other faults (e.g., Becken & Ritter, 2011). At near-surface depths (<5 km), low-resistivity anomalies are coincident with the fault locations and can be attributed to a crush zone and circulating meteoric fluids. However, at greater depths the fault system appears to have been sealed by compaction processes, because no lower crustal fluid drainage is imaged, despite the fault system's proximity to fluid-rich domains. Thus, in the midcrust the fault may be dry (e.g., Unsworth & Rondenay, 2012), in agreement with the frequency of large slip events, which have occurred on timescales of thousands of years (Rizza et al., 2015), although detailed microseismicity has not been reported.

Furthermore, patterns of compaction-induced localization are imposed on tectonic deformation and lithological structure (e.g., Connolly & Podladchikov, 2013). These effects may explain the elongation of the low-resistivity domains orthogonal to the 2-D resistivity models and quasi-parallel to the adjacent fault zone (see Käufl et al., 2020; Figure S5).

4. Conclusions

Images of the electrical resistivity structure below the intracontinental Bulnay region, north central Mongolia, reveal discrete low-resistivity zones (<30 Ωm; ~25 km wide) in the lower crust that have a characteristic pattern. These features are believed to be laterally extended structures that are quasi-parallel to the adjacent fault zone and perpendicular to tectonic stress from northward directed compression. The low-resistivity zones are determined to be compatible with a conceptual model of compaction-induced localization and stagnation of metamorphic fluids. The conceptual model predicts that fluids released in the lower crust will collect in oblate zones ~9 km below the BDTZ, in agreement with the electrical resistivity models. A further demonstration of the consistency of the compaction model comes from plausible values of 270–360 kJ/mol for the activation energy, suggesting the viscous mechanism is dislocation creep. The electrical resistivity models constrain the lower crustal viscous compaction length to be on the order of 10 km in the Bulnay region. A compaction length of this magnitude is consistent with estimates for the relevant

hydraulic and rheological properties. The results discussed here imply that tectonic and compaction processes, rather than lithological-structural heterogeneity, control lower crustal fluid flow.

Data Availability Statement

The MT data are archived by the German Research Centre for Geosciences (GFZ) Potsdam. They can be freely accessed with the Data Services portal through the GIPP Experiment Database by navigating to http://gipp.gfz-potsdam.de/projects/view/545 website. Additional explanatory details can be obtained in the supporting information document.

Acknowledgments

This research was financially supported by the DFG (Grant BE5149/6-1) and the SNF (Grant 200021L_162660/1). M. B. is funded through a DFG Heisenberg Grant (5149/7-1 and 5149/9-1). We thank Kerry Key for providing the MT inversion code. We thank the Geophysical Instrument Pool Potsdam (GIPP) for providing MT instruments (application #201613). We thank all those who helped collect the data and provided support, especially Johannes Käufl and Jochen Kamm, as well as our colleagues from the Institute of Astronomy and Geophysics of the Mongolian Academy of Sciences.

References

Badarch, G., Cunningham, W. D., & Windley, B. F. (2002). A new subdivision for Mongolia: Implications for the Phanerozoic crustal growth of Central Asia. *Journal of Asian Earth Science*, *21*(1), 87–110. https://doi.org/10.1016/S1367-9120(02)00017-2

Barry, T. L. (1999). Origins of Cenozoic basalts in Mongolia: Chemical and isotope study (doctoral dissertation). From University of Leicester Department of Geology. Leicester, United Kingdom: University of Leicester.

Barry, T. L., Saunders, A. D., Kempton, P. D., Windley, B. F., Pringle, M. S., Dorjnamjaa, D., & Saandar, S. (2003). Petrogenesis of Cenozoic basalts from Mongolia: Evidence for the role of asthenospheric versus metasomatized lithospheric mantle sources. *Journal of Petrology*, *44*(1), 55–91. https://doi.org/10.1093/petrology/44.1.55

Beard, D. E., & Weyl, P. K. (1973). Influence of texture on porosity and permeability of unconsolidated sand. *Bulletin of the American Association of Petroleum Geologists*, *57*, 349–369. https://doi.org/10.1306/819A4272-16C5-11D7-8645000102C1865D

Becken, M., & Burkhardt, H. (2004). An ellipticity criterion in magnetotelluric tensor analysis. *Geophysical Journal International*, *159*(1), 69–82. https://doi.org/10.1111/j.1365-246X.2004.02376.x

Becken, M., & Ritter, O. (2011). Magnetotelluric studies at the San Andreas Fault zone: Implications for the role of fluids. *Surveys in Geophysics*, *33*(1), 65–105. http://doi.org/10.1007/s10712-011-9144-0

Becken, M., Ritter, O., Bedrosian, P. A., & Weckmann, U. (2011). Correlation between deep fluids, tremor and creep along the central San Andreas fault. *Nature*, *480*(7375), 87–90. https://doi.org/10.1038/nature10609

Booker, J. (2014). The magnetotelluric phase tensor: A critical review. *Surveys in Geophysics*, *35*, 7–40. http://doi.org/10.1007/s10712-013-9234-2

Bürgmann, R., & Dresen, G. (2008). Rheology of the lower crust and upper mantle: Evidence from rock mechanics, geodesy, and field observations. *Annual Review of Earth and Planetary Sciences*, *36*(1), 531–567. https://doi.org/10.1146/annurev.earth.36.031207.124326

Calais, E., Vernolle, M., San'kov, V., Lukhnev, A., Miroshnitchenko, A., Amarjargal, S., & Déverchère, J. (2003). GPS measurements of crustal deformation in the Baikal–Mongolia area (1994–2002): Implications for current kinematics of Asia. *Journal of Geophysical Research*, *108*(B10), 2501. https://doi.org/10.1029/2002JB002373

Caldwell, T. G., Bibby, H. M., & Brown, C. (2004). The magnetotelluric phase tensor. *Geophysical Journal International*, *158*(2), 457–469. https://doi.org/10.1111/j.1365-246X.2004.02281.x

Carman, P. C. (1939). Permeability of saturated sands, soils and clays. *Journal of Agricultural Science*, *29*(2), 262–273. https://doi.org/10.1017/S0021859600051789

Chave, A. D., & Jones, A. G. (Eds) (2012). *The magnetotelluric method: Theory and practice*. Cambridge: Cambridge University Press. https://doi.org/10.1017/CBO9781139020138

Comeau, M. J. (2015). Electrical resistivity structure of the Altiplano-Puna magma body and volcan uturuncu from magnetotelluric data. (PhD Dissertation). Edmonton, Canada: University of Alberta. https://doi.org/10.7939/R3C24QW2S

Comeau, M. J., Becken, M., Käufl, J. S., Grayver, A. V., Kuvshinov, A. V., Tserendug, S., et al. (2020). Evidence for terrane boundaries and suture zones across Southern Mongolia detected with a 2-dimensional magnetotelluric transect. *Earth, Planets and Space*, *72*(5), 1–13. https://doi.org/10.1186/s40623-020-1131-6

Comeau, M. J., Käufl, J. S., Becken, M., Kuvshinov, A. V., Grayver, A. V., Kamm, J., et al. (2019). Mineralization of the Bayankhongor Metal Belt and the South Hangai suture zone, Mongolia: Insights from 3-D electrical resistivity models. *Proceedings of the 28th Schmucker-Weidelt Colloquium for Electromagnetic Depth Research*, Haltern am see, Germany, September, 2019.

Comeau, M. J., Käufl, J. S., Becken, M., Kuvshinov, A. V., Grayver, A. V., Kamm, J., et al. (2018). Evidence for fluid and melt generation in response to an asthenospheric upwelling beneath the Hangai Dome, Mongolia. *Earth and Planetary Science Letters*, *487*, 201–209. https://doi.org/10.1016/j.epsl.2018.02.007

Comeau, M. J., Unsworth, M. J., & Cordell, D. (2016). New constraints on the magma distribution and composition beneath Volcán Uturuncu and the southern Bolivian Altiplano from magnetotelluric data. *Geosphere*, *12*(5), 1391–1421. https://doi.org/10.1130/GES01277.1

Connolly, J. A. D. (1997). Devolatilization-generated fluid pressure and deformation-propagated fluid flow during prograde regional metamorphism. *Journal of Geophysical Research*, *102*(B8), 18149–18173. https://doi.org/10.1029/97JB00731

Connolly, J. A. D. (2010). The mechanics of metamorphic fluid expulsion. *Elements*, *6*(3), 165–172. https://doi.org/10.2113/gselements.6.3.165

Connolly, J. A. D., & Podlachikov, Y. Y. (2004). Fluid flow in compressive tectonic settings: Implications for midcrustal seismic reflectors and downward fluid migration. *Journal of Geophysical Research*, *109*, B04201. https://doi.org/10.1029/2003JB002822

Connolly, J. A. D., & Podladchikov, Y. Y. (1998). Compaction-driven fluid flow in viscoelastic rock. *Geodinamica Acta*, *11*(2–3), 55–84. https://doi.org/10.1080/09853111.1998.11105311

Connolly, J. A. D., & Podladchikov, Y. Y. (2013). A hydromechanical model for lower crustal fluid flow. In D. E. Harlov & H. Austrheim (Eds.), *Metasomatism and the chemical transformation of rock* (pp. 599–658). Berlin: Springer. https://doi.org/10.1007/978-3-642-28394-9_14

Connolly, J. A. D., Schmidt, M. W., Solferino, G., & Bagdassarov, N. (2009). Permeability of asthenospheric mantle and melt extraction rates at mid-ocean ridges. *Nature*, *462*(7270), 209–212. https://doi.org/10.1038/nature08517

Cox, S. F. (1999). Deformational controls on the dynamics of fluid flow in mesothermal gold systems. In K. McCaffrey (Ed.), *Fractures, fluid flow and mineralization* (pp. 123–140). London: Geological Society Special Publications. https://doi.org/10.1144/GSL.SP.1999.155.01.10

Cunningham, W. D. (2001). Cenozoic normal faulting and regional doming in the southern Hangay region, Central Mongolia: Implications for the origin of the Baikal rift province. *Tectonophysics*, *331*(4), 389–411. https://doi.org/10.1016/S0040-1951(00)00228-6

Déverchère, J., Petit, C., Gileva, N., Radziminovitch, N., Melnikova, V., & Sankov, V. (2001). Depth distribution of earthquakes in the Baikal rift system and its implications for the rheology of the lithosphere. *Geophysical Journal International*, *146*(3), 714–730. https://doi.org/10.1046/j.0956-540x.2001.1484.484.x

Eisel, M., & Haak, V. (1999). Macro-anisotropy of the electrical conductivity of the crust: A magnetotelluric study from the German Continental Deep Drilling site (KTB). *Geophysical Journal International*, *136*(1), 109–122. https://doi.org/10.1046/j.1365-246X.1999.00707.x

Hack, A., & Thompson, A. (2011). Density and viscosity of hydrous magmas and related fluids and their role in subduction zone processes. *Journal of Petrology*, *52*(7–8), 1333–1362. https://doi.org/10.1093/petrology/egq048

Hashin, Z., & Shtrikman, S. (1962). A variational approach to the theory of the effective magnetic permeability of multiphase materials. *Journal of Applied Physics*, *33*(10), 3125–3131. https://doi.org/10.1063/1.1728579

Heise, W., & Pous, J. (2001). Effects of anisotropy on the two-dimensional inversion procedure. *Geophysical Journal International*, *147*(3), 610–621. https://doi.org/10.1046/j.0956-540x.2001.01560.x

Hunt, A. C., Parkinson, I. J., Harris, N., Barry, T. L., Rogers, N. W., & Yondon, M. (2012). Cenozoic volcanism on the Hangai Dome, Central Mongolia: Geochemical evidence for changing melt sources and implications for mechanisms of melting. *Journal of Petrology*, *53*(9), 1913–1942. https://doi.org/10.1093/petrology/egs038

Hyndman, R. D., Vanyan, L. L., Marquis, O., & Law, L. K. (1993). The origin of electrically conductive lower continental crust: Saline water or graphite? *Physics of the Earth and Planetary Interiors*, *81*(1–4), 325–345. https://doi.org/10.1016/0031-9201(93)90139-Z

Ionov, D. (2002). Mantle structure and rifting processes in the Baikal–Mongolia region: Geophysical data and evidence from xenoliths in volcanic rocks. *Tectonophysics*, *351*(1–2), 41–60. https://doi.org/10.1016/S0040-1951(02)00124-5

Ionov, D. A., O'Reilly, S. Y., & Griffin, W. L. (1998). A geotherm and lithospheric section for central Mongolia (Tariat Region). In M. F. J. Flower, S.-L. Chung, C.-H. Lo, T.-Y. Lee (Eds.), *Mantle dynamics and plate interaction in East Asia* (pp. 127–153). Washington, DC: American Geophysical Union. https://doi.org/10.1029/GD027p0127

Karato, S. (2008). *Deformation of Earth materials: An introduction to the rheology of solid Earth*. Cambridge: Cambridge University Press. https://doi.org/10.1017/CBO9780511804892

Käufl, J. S., Grayver, A. V., Comeau, M. J., Kuvshinov, A. V., Becken, M., Batmagnai, E., & Demberel, S. (2020). Magnetotelluric multiscale 3-D inversion reveals crustal and upper mantle structure beneath the Hangai and Gobi-Altai region in Mongolia. *Geophysical Journal International*, *22*. https://doi.org/10.1093/gji/ggaa039

Kestin, J., Khalifa, H. E., & Correia, R. J. (1981). Tables of the dynamic and kinematic viscosity of aqueous NaCl solutions in the temperature range 20–150°C and the pressure range 0.1–35 MPa. *Journal of Physical and Chemical Reference Data*, *10*(1), 71–88. https://doi.org/10.1063/1.555641

Key, K. (2016). MARE2DEM: A 2-D inversion code for controlled-source electromagnetic and magnetotelluric data. *Geophysical Journal International*, *207*(1), 571–588. https://doi.org/10.1093/gji/ggw290

Li, C. F., Ly, Y., & Wang, J. (2017). A global reference model of Curie-point depths based on EMAG2. *Scientific Reports*, *7*. https://doi.org/10.1038/srep45129

Liddell, M., Unsworth, M., & Pek, J. (2016). Magnetotelluric imaging of anisotropic crust near Fort McMurray, Alberta: Implications for engineered geothermal system development. *Geophysical Journal International*, *205*(3), 1365–1381. https://doi.org/10.1093/gji/ggw089

Manning, C. (2018). Fluids of the lower crust: Deep is different. *Annual Review of Earth and Planetary Sciences*, *46*(1), 67–97. https://doi.org/10.1146/annurev-earth-060614-105224

Marti, A. (2014). The role of electrical anisotropy in magnetotelluric responses: From modelling and dimensionality analysis to inversion and interpretation. *Surveys in Geophysics*, *35*(1), 179–218. https://doi.org/10.1007/s10712-013-9233-3

Paterson, M. S., & Luan, F. C. (1990). Quartzite rheology under geological conditions. In R. J. Knipe & E. H. Rutter (Eds.), *Deformation mechanisms, rheology and tectonics* (pp. 299–307). Cambridge: Geological Society Special Publications. https://doi.org/10.1144/GSL.SP.1990.054.01.26

Pek, J., & Verner, T. (1997). Finite-difference modelling of magnetotelluric fields in two-dimensional anisotropic media. *Geophysical Journal International*, *128*(3), 505–521. https://doi.org/10.1111/j.1365-246X.1997.tb05314.x

Petit, C., Tiberi, C., Deschamps, A., & Deverchere, J. (2008). Teleseismic traveltimes, topography and the lithospheric structure across central Mongolia. *Geophysical Research Letters*, *35*, 1–5.

Pommier, A., & Le Trong, E. (2011). SIGMELTS: A web portal for electrical conductivity calculations in geosciences. *Computational Geosciences*, *37*, 1450–1459. https://doi.org/10.1016/j.cageo.2011.01.002

Priestley, K., Debayle, E., McKenzie, D., & Pilidou, S. (2006). Upper mantle structure of eastern Asia from multimode surface waveform tomography. *Journal of Geophysical Research*, *111*.

Pritchard, M. E., de Silva, S. L., Michelfelder, G., Zandt, G., McNutt, S. R., Gottsmann, J., et al. (2018). Synthesis: PLUTONS: Investigating the relationship between pluton growth and volcanism in the Central Andes. *Geosphere*, *14*(3), 954–982. https://doi.org/10.1130/GES01578.1

Rizza, M., Ritz, J. F., Prentice, C., Vassalo, R., & Braucher, R. (2015). Earthquake geology of the Bulnay Fault (Mongolia). *Bulletin of the Seismological Society of America*, *105*, 72–93. https://doi.org/10.1785/0120140119

Rosenberg, C. L., & Handy, M. R. (2005). Experimental deformation of partially melted granite revisited: Implications for the continental crust. *Journal of Metamorphic Geology*, *23*, 19–28. https://doi.org/10.1111/j.1525-1314.2005.00555.x

Sakuma, H., & Ichiki, M. (2016). Electrical conductivity of NaCl-H_2O fluid in the crust. *Journal of Geophysical Research: Solid Earth*, *121*, 577–594. https://doi.org/10.1002/2015JB012219

Scott, D. R., & Stevenson, D. J. (1984). Magma solitons. *Geophysical Research Letters*, *1*, 1161–1164. https://doi.org/10.1029/GL011i011p01161

Sibson, R. H. (1986). Earthquakes and rock deformation in crustal fault zones. *Annual Review of Earth and Planetary Sciences*, *14*(1), 149–175. https://doi.org/10.1146/annurev.ea.14.050186.001053

Sinmyo, R., & Keppler, H. (2017). Electrical conductivity of NaCl-bearing aqueous fluids to 600 C and 1 GPa. *Contributions to Mineralogy and Petrology*, *172*(1), 4. https://doi.org/10.1007/s00410-016-1323-z

Unsworth, M. J., & Rondenay, S. (2012). Mapping the distribution of fluids in the crust and lithospheric mantle utilizing geophysical methods. In D. E. Harlov & H. Austrheim (Eds.), *Metasomatism and the chemical transformation of rock, lecture notes in Earth system sciences* (pp. 535–598). Berlin: Springer. http://doi.org/10.1007/978-3-642-28394-9_13

Vergnolle, M., Pollitz, F., & Calais, E. (2003). Constraints on the viscosity of the continental crust and mantle from GPS measurements and postseismic deformation models in western Mongolia. *Journal of Geophysical Research*, *108*(B10), 2502. https://doi.org/10.1029/2002JB002374

Walker, R. T., Nissen, E., Molor, E., & Bayasgalan, A. (2007). Reinterpretation of the active faulting in central Mongolia. *Geology*, *35*(8), 759–762. https://doi.org/10.1130/G23716A.1

Watanabe, T. (1993). Effects of water and melt on seismic velocities and their application to characterization of seismic refelctors. *Geophysical Research Letters*, *20*(24), 2933–2936. https://doi.org/10.1029/93GL03170

Welkey, J., Meltzer, A., Stachnik, J., Munkhuu, U., Tsagaan, B., & Russo, R. (2018). Intracontinental deformation and crustal structure: Hangay Dome, Central Mongolia. *American Geophysical Union Fall Meeting*, Washington, U.S.A, December, 2018,

Wilkinson, D. S., & Ashby, M. F. (1975). Densification of porous materials by power-law creep. *Acta Metallurgica*, *23*(11), 1277–1285. https://doi.org/10.1016/0001-6160(75)90136-4

Yin, A. (2010). Cenozoic evolution of Asia: A preliminary synthesis. *Tectonophysics*, *488*(1–4), 293–325. https://doi.org/10.1016/j.tecto.2009.06.002